$BaHfO_3$-Doped Thick $YBa_2Cu_3O_{7-\delta}$ Films on Highly Alloyed Textured Ni-W Tapes

Max Sieger, Jens Hänisch, Patrick Pahlke, Maria Sparing, Uwe Gaitzsch, Kazumasa Iida, Rainer Nast, Elke Reich, Ludwig Schultz, Bernhard Holzapfel, and Ruben Hühne

***Abstract*—$\mathbf{YBa_2Cu_3O_{7-\delta}}$ (YBCO) films with a thickness of up to 2 μm containing nano-sized $\mathbf{BaHfO_3}$ (BHO) have been grown on biaxially textured metal tapes by pulsed laser deposition. Transmission electron microscopy revealed the inclusion of $\mathbf{Y_2O_3}$ platelets and rod-like BHO structures. A *c*-axis oriented growth of the YBCO layer and biaxial oriented incorporation of BHO is confirmed by X-Ray diffraction. BHO expands the *c*-axis of YBCO, flattens the surface of YBCO and densifies the films. $\mathbf{Y_2O_3}$ inclusions get smaller and finer distributed, possibly with a positive influence on pinning effects. A superconducting transition temperature T_c of about 89 K was determined, decreasing slightly with increasing BHO content. Transport current measurements in the maximum Lorentz force configuration showed an increased irreversibility field H_{irr} and higher pinning force density F_p with increasing BHO content in high magnetic fields.**

***Index Terms*—BHO, pinning, pulsed laser deposition, RABiTS, YBCO.**

I. Introduction

$YBa_2Cu_3O_{7-\delta}$ (YBCO) is one of the desired high-temperature superconductors (HTS) in technical applications such as superconducting transmission cables, motors and electrical power components due to its superior current transport capability in high magnetic fields [1]. The recent need for large amounts of superconducting tape is targeted by coated conductor (CC) technologies, i.e., deposition of HTS on textured metal tapes [2]. Ni-W tapes are highly formable and have a good texture formation and thermal stability [3], [4]. Increasing the amount of tungsten lowers the Curie temperature to below 77 K in Ni-9at% W (Ni9W) [5]. Such tapes can be used as non-magnetic CC substrates with reduced AC losses at working temperature [5], [6]. Cube texture in the tape can be realized by heavy cold rolling and annealing (RABiTS) [5] and is transferred through a buffer layer system to the superconducting layer [7]. For applications at medium and high magnetic fields, e.g., rotating machines, superconducting energy storage devices and magnets, improved pinning is necessary to immobilize magnetic flux lines in the superconductor to increase $J_c(B)$ [8]–[14]. $BaHfO_3$ (BHO) nanoparticles are an effective option for artificial pinning centers [15].

The critical current I_c a CC can carry is also depending on the thickness of the superconducting layer [16], therefore the trend is to grow thicker films for high-I_c applications. Here, we show BHO-doped YBCO (BHO:YBCO) films with a thickness of $\sim$2 μm grown by pulsed laser deposition (PLD) on single crystalline $SrTiO_3$ (STO) and technical substrates as a promising way to improve the performance of CCs.

II. Experimental Details

A. Sample Preparation

BHO:YBCO films were prepared by PLD of 0, 2, 4, and 6 mol% BHO-doped YBCO targets. A *Lambda Physics LPX305i* KrF excimer laser ($\lambda = 248$ nm, $t_{pulse} = 25$ ns) was used with an energy density of 1.6 J/cm^2 at the PLD target surface to grow BHO:YBCO on 10 mm $\times$ 10 mm pieces of 80 μm thick cube-textured (96 % fraction of cube texture ($< 10^\circ$) [6]) Ni9W tapes with a PLD-Y_2O_3/YSZ/CeO_2 buffer layer stack on top as well as on STO. The details of the tape preparation and buffer layer deposition may be found in [7] and [16]. An oxygen partial pressure of 0.4 mbar was maintained during the deposition process. The deposition temperature was set to 830 °C, which was found optimum for deposition of BHO:YBCO films with high critical temperatures, T_c, and critical current densities, J_c, in previous experiments. *In-situ* oxygen loading of the YBCO films took place in 400 mbar O_2 during cooling at 20 K min^{-1} to obtain superconducting YBCO.

B. Structural Characterization

Surface morphology and film thickness were analyzed by scanning electron microscopy using an *FEI Helios Nanolab 600i* to cut cross sections by a focused gallium ion beam. Transmission electron microscopy (TEM) analysis was carried out with a *FEI Tecnai G²* (LaB_6 cathode, 200 kV). X-Ray diffraction in Bragg-Brentano geometry was carried out on a *Bruker D8 Advance* with a Co anode (Θ-2Θ-scans). The length of the *c*-axis lattice parameter was calculated by applying the Nelson-Riley formula [17] to the YBCO (00ℓ) peak positions. The BHO lattice parameter was calculated from the 2Θ-position of the BHO (004) maximum peak intensity in the

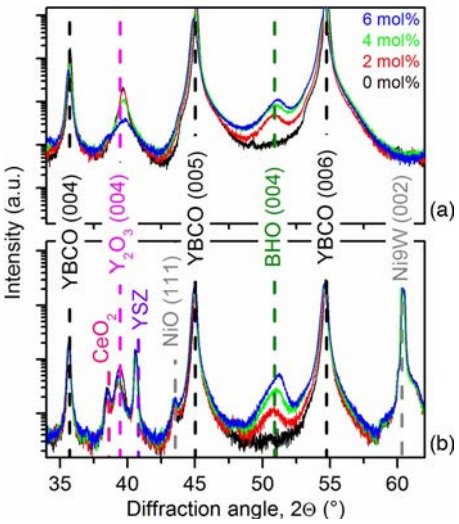

Fig. 1. XRD patterns of BHO:YBCO films with different amounts of BHO on (a) STO and (b) Ni9W tape. Both patterns show c-axis oriented growth of YBCO and BHO. With increasing BHO content the BHO (004) intensity increases, the peak maximum slightly shifts and the Y_2O_3 (004) intensity decreases (on Ni9W tape overlapped by a Y_2O_3 buffer layer).

corresponding Θ-2Θ-scans. Pole figures of metal tape, buffer layers, YBCO and BHO were measured at a *Philips X'Pert PW3040* with a Cu anode.

C. Electrical Properties

The critical temperature T_c (defined at midpoint of transition) and the transition width ΔT_c were determined by inductively measuring the appearance of shielding currents in the films. Bridges of 800 μm length and 500 μm width for transport current measurements on Ni9W substrates were prepared by laser cutting [18]. Field dependencies of the critical current density, $J_c(B)$, in magnetic fields up to 9 T were measured in a four point probe assembly with a *Quantum Design physical properties measurement system* (PPMS) via $V(I)$ curves with an electrical field criterion of 1 μV/cm. Pinning force densities were calculated by $F_P = J_c \cdot B$ and H_{irr} values were estimated from the empirical fits to the pinning force curves at high magnetic fields.

III. Results and Discussion

A. Structural Properties

The YBCO matrix and the cubic BHO ($a = 8.333$ Å [19]) grow c-axis oriented on STO and on Ni9W tape. This is confirmed by the appearance of only (00ℓ) peaks in the Θ-2Θ scans, Fig. 1. On both substrates the BHO (004) peak height is increasing with BHO concentration, its position is slightly moving to higher angles, indicating a shortening of the average BHO lattice parameters (cf. Fig. 2(b)).

In films on Ni9W, the Y_2O_3 (004) [20] peak is dominated by the Y_2O_3 buffer layer. Therefore only the Y_2O_3 (004) peak for films on STO can be evaluated. A decrease of the peak height and an increase of their FWHM (full width at half maximum) with increasing BHO content corresponds to a smaller amount and a finer distribution of the Y_2O_3 platelets (cf. Fig. 3). The

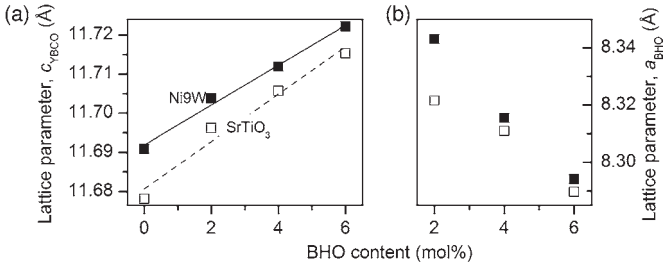

Fig. 2. Lattice constants of (a) YBCO c-axis and (b) BHO of BHO:YBCO films on STO and Ni9W. BHO elongates the lattice constant. Compressive strain in the YBCO ab-plane from thermal shrinkage of the metal tape additionally elongates c_{YBCO} on Ni9W. The symbol size indicates the uncertainty of the Nelson-Riley fit.

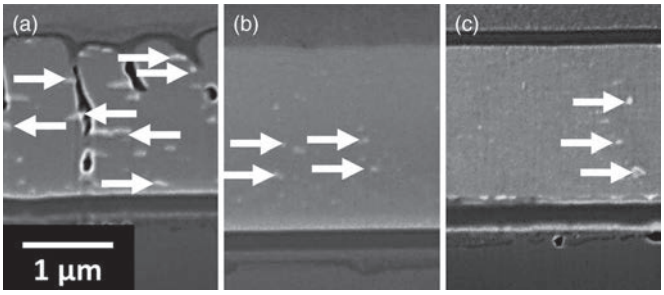

Fig. 3. Cross section SEM images of (a) YBCO, (b) 2 mol% BHO:YBCO, (c) 6 mol% BHO:YBCO films on Ni9W, Y_2O_3 is marked by white arrows. The scale bar is the same for all pictures.

total amount of Y_2O_3, estimated by the area under the peak, is nearly constant for 2 mol% BHO and decreases for 4 mol% (-16%) and 6 mol% BHO (-43%). We suggest that Yttrium is incorporated into BHO, as has been observed for $BaZrO_3$ and $BaNbO_3$ [11].

An elongation of the c-axis lattice parameter of YBCO by increasing BHO content is shown in Fig. 2(a). The c-axis increases proportional to the BHO concentration due to strain effects on the YBCO matrix [21]. On STO the ab-plane of YBCO is widened to match the substrate lattice parameters ($a_{STO} = 3.905$ Å) resulting in a smaller c-axis compared to films on Ni9W. A large thermal shrinkage of the metal tape after deposition induces compressive strain in the ab-plane and elongates the c-axis. The c-axis dependencies of YBCO on STO and Ni9W are fitted linearly. Considering the uncertainty of the Nelson-Riley fit due to the influence of the oxygen deficiency δ on the peak positions, the two slopes might be the same (~ 0.005 Å/mol%). In comparison the lattice parameter of BHO is shrinking with increasing BHO content (Fig. 2(b)).

SEM pictures of cross sections, Fig. 3, show a densification and flattening of the YBCO surface by even 2 mol% BHO as well as a finer distribution of precipitates. The same trend is observed for BHO:YBCO films on STO. The absence of large Y_2O_3 precipitates inducing macroscopic pores during growth (cf. Fig. 3(a): each pore seems to start on top of a precipitate) might lead to the improved microstructure.

Fig. 4(a) shows a schematic draft of the different unit cell orientations in our CC architecture with the measured lattice planes and explains the tilt between the different pole figures. Pole figures of the Ni (111), Fig. 4(b), BHO (101), Fig. 4(c), YBCO (102), Fig. 4(d), and YSZ (111), Fig. 4(e), lattice

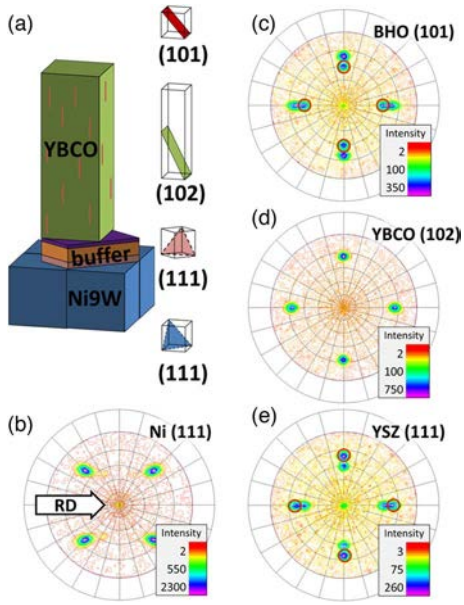

Fig. 4. (a) Schematic illustration of unit cell orientations in a Ni9W/Y_2O_3/YSZ/CeO_2/BHO:YBCO CC architecture. Drafted lattice planes accompany the pole figures of (b) Ni (111), (c) BHO (101), (d) YBCO (102), (e) YSZ (111) for 6 mol% BHO:YBCO on Y_2O_3/YSZ/CeO_2-buffered Ni9W. Rolling direction of the tape is marked in (b). The BHO (101) and YSZ (111) lattice planes have similar 2Θ angles and occur in both pole figures (c) and (e). The respective peaks are marked by red circles.

planes indicate that all layers grow epitaxially and that BHO is biaxially oriented within the matrix (shown for 6 mol% BHO:YBCO). Pole figures of samples with other doping contents are similar in appearance and FWHM values and show an increase in maximum intensity comparable to Fig. 1. BHO doping up to 6 mol% has no effect on the texture of YBCO in our experiments.

The elliptical shape of most of the peaks is due to the recrystallization texture of the metal tape. The vicinity of the 2Θ angles for YSZ (111) $(2\Theta = 30.08^\circ)$ and BHO (101) $(2\Theta = 30.33^\circ)$ is the reason for the appearance of one plane in the pole figure of the respective other.

The CC architecture was analyzed by TEM for the 2 mol% BHO:YBCO sample. The buffer architecture consists of ∼130 nm Y_2O_3, ∼210 nm YSZ, and ∼30 nm CeO_2 and shows flat and dense interfaces, Fig. 5(a). BHO is mostly incorporated as nanorods and occasionally as nanoparticles into the YBCO matrix, see white arrows in Fig. 5(b). The formation of nanorods is diffusion driven and depends critically on deposition temperature and secondary-phase amount: at lower deposition temperatures more and thinner nanorods [22] and/or nanoparticles [23] are formed whereas at higher deposition temperatures they tend to grow fewer but thicker [22]. For 2 mol% BHO content (∼1 wt%) of the films the nanorods have a diameter of about 6–7 nm and a distance of 35–40 nm (Fig. 5(b)). The nanorods grow along the YBCO c-axis direction with a relatively large angular splay of $\sim 20^\circ$ and typical lengths of 50–300 nm. This splay as well as the combination of nanorods and nanoparticles is advantageous for pinning properties since it prevents flux line hopping due to double-kink structures [24]. The appearance of Y_2O_3 platelets parallel to the ab-plane of YBCO is shown in Fig. 5(c).

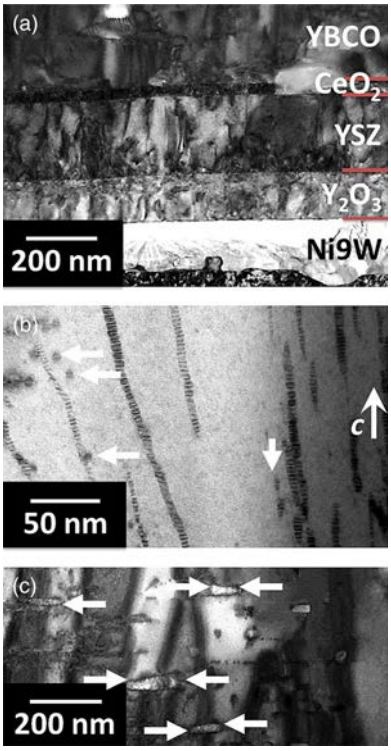

Fig. 5. TEM images of 2 mol% BHO:YBCO on Ni9W (a) CC architecture, (b) c-axis oriented nanorods of BHO (white arrows mark BHO nanoparticles), (c) Y_2O_3 platelets in the ab-plane.

TABLE I
FILM THICKNESS, $T_{c,50}$, ΔT_c, AND H_{irr} (77 K), OF BHO:YBCO FILMS ON NI9W

BHO (mol%)	Thickness (μm)	$T_{c,50}$ (K)	ΔT_c (K)	H_{irr} (T)
0	1.8	89.1	1.0	7.2
2	2.1	88.1	0.8	7.6
4	2.0	88.5	0.7	9.1
6	1.8	87.7	0.9	10.3

B. Electrical Properties

Table I gives the film thickness, transition temperature, $T_{c,50}$, transition width, ΔT_c, and irreversibility field at 77 K, H_{irr} for the BHO:YBCO films on Ni9W. The respective critical current density, $J_c(B)$, and pinning force density curves at 77 K are given in Fig. 6. Despite a slight decrease in T_c, Table I, the addition of BHO clearly increases the critical current densities in high magnetic fields, Fig. 6(a). At low magnetic fields, in contrast, J_c is nearly independent of BHO concentration. The reason is the J_c limitation by grain boundaries (GB) (weak-link behavior) [25], [26]. Besides the well-known GB angle dependence of J_c, the YBCO grains are sometimes only poorly connected at the underlying grain boundaries of the Ni tapes, cf. Fig. 4(a) in Ref. [7]. To estimate the possible effect of BHO at low fields, the pinning force density F_p, Fig. 6(b), was fitted in the high-field part with the empirical field dependence

$$F_p \sim (H/H_{irr})^p (1 - H/H_{irr})^q. \quad (1)$$

Although the F_p curves (dashed lines) are only rough estimates and the actual curves might be more complex

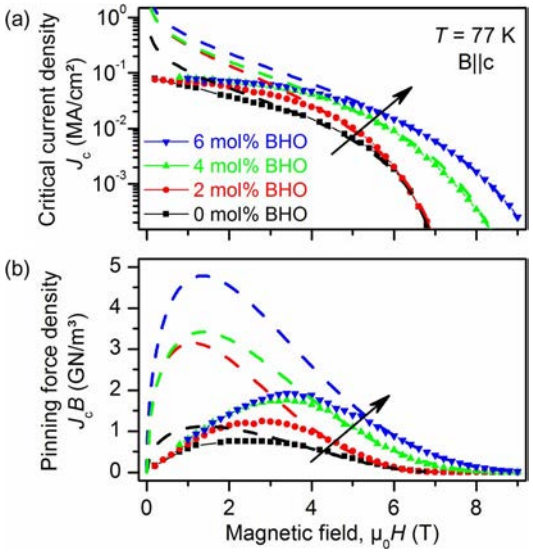

Fig. 6. Field dependence of (a) the critical current density and (b) the pinning force density for YBCO films with different BHO content on Ni9W. Dashed lines are fits according to Eq. (1). BHO increases the critical current density and pinning force density in high magnetic fields (> 4 T). The low field region is mainly limited by grain boundaries, resulting in decreased J_c values.

(cf. e.g., Fig. 3 in [20]), they show a clear trend of increasing pinning forces and irreversibility fields with increasing BHO content, Table I. The crossover field between GB limitation and pinning limitation depends both on texture quality [24], [25] and pinning force density within the grains. The higher the intra-grain ability to pin the flux lines for a given film with a certain grain boundary network, the higher is the crossover field.

IV. Conclusion

High-quality thick YBCO films with BHO addition of up to 6 mol% have been grown on Ni9W tapes. All layers grow epitaxially; BHO is incorporated with biaxial texture as nanorods and nanoparticles in the YBCO matrix. BHO contents up to 6 mol% improve J_c in high magnetic fields. The maximum has not yet been reached, a further increase in H_{irr} and F_{p} is possible by higher BHO contents. At low magnetic fields, J_{c} is limited by grain boundary weak links and, therefore, unaffected by BHO addition. To increase J_{c} in this field region, the quality of the grain boundaries has to be improved.

Acknowledgment

The authors gratefully acknowledge C. Rodig, J. Scheiter, U. Fiedler, and M. Kühnel for technical assistance.

References

[1] S. Foltyn *et al.*, "Materials science challenges for high-temperature superconducting wire," *Nat. Mater.*, vol. 6, no. 9, pp. 631–642, Sep. 2007.

[2] X. Obradors and T. Puig, "Coated conductors for power applications: Materials challenges," *Supercond. Sci. Technol.*, vol. 27, no. 4, Mar. 2014, Art. ID. 044003.

[3] E. Specht *et al.*, "Cube-textured nickel substrates for high-temperature superconductors," *Supercond. Sci. Technol.*, vol. 11, no. 10, pp. 945–949, Feb. 1998.

[4] J. Eickemeyer, D. Selbmann, R. Optiz, E. Maher, and W. Prusseit, "Effect of nickel purity on cube texture formation in RABiT-tapes," *Phys. C, Supercond.*, vol. 341–348, pp. 2425–2426, Nov. 2000.

[5] U. Gaitzsch *et al.*, "Highly alloyed Ni-W substrates for low AC loss applications," *Supercond. Sci. Technol.*, vol. 26, no. 8, Jul. 2013, Art. ID. 085024.

[6] J. Eickemeyer *et al.*, "Textured Ni-9.0% W substrate tapes for YBCO-coated conductors," *Supercond. Sci. Technol.*, vol. 23, no. 8, Jul. 2010, Art. ID. 085012.

[7] R. Hühne *et al.*, "Preparation of coated conductor architectures on Ni composite tapes," *Supercond. Sci. Technol.*, vol. 20, no. 7, pp. 709–714, Jun. 2007.

[8] T. Matsushita, "Flux pinning in superconducting 123 materials," *Supercond. Sci. Technol.*, vol. 13, no. 6, pp. 730–737, Feb. 2000.

[9] T. Haugan, P. N. Barnes, R. Wheeler, F. Meisenkothen, and M. Sumption, "Addition of nanoparticle dispersions to enhance flux pinning of the $YBa_2Cu_3O_{7-x}$ superconductor," *Nature*, vol. 430, no. 7002, pp. 867–870, Aug. 2004.

[10] K. Matsumoto and P. Mele, "Artificial pinning center technology to enhance vortex pinning in YBCO coated conductors," *Supercond. Sci. Technol.*, vol. 23, no. 1, Dec. 2009, Art. ID. 014001.

[11] E. Reich *et al.*, "Structural and pinning properties of $Y_2Ba_4CuMO_y$ $(M = Nb, Zr)/YBa_2Cu_3O_{7-\delta}$ quasi-multilayers fabricated by off-axis pulsed laser deposition," *Supercond. Sci. Technol.*, vol. 22, no. 10, Aug. 2009, Art. ID. 105004.

[12] A. Goyal *et al.*, "Irradiation-free, columnar defects comprised of self-assembled nanodots and nanorods resulting in strongly enhanced flux-pinning in $YBa_2Cu_3O_{7-\delta}$ films," *Supercond. Sci. Technol.*, vol. 18, no. 11, pp. 1533–1538, Oct. 2005.

[13] J. MacManus-Driscoll *et al.*, "Strongly enhanced current densities in superconducting coated conductors of $YBa_2Cu_3O_{7-x} + BaZrO_3$," *Nat. Mater.*, vol. 3, no. 7, pp. 439–443, Jul. 2004.

[14] J. Hänisch *et al.*, "Formation and pinning properties of growth-controlled nanoscale precipitates in $YBa_2Cu_3O_{7-\delta}$/transition metal quasi-multilayers," *Supercond. Sci. Technol.*, vol. 19, no. 6, pp. 534–540, Apr. 2006.

[15] A. Tsuruta *et al.*, "Flux pinning properties at low temperatures in $BaHfO_3$ doped $SmBa_2Cu_3O_y$ films," *IEEE Trans. Appl. Supercond.*, vol. 23, no. 3, Jun. 2013, Art. ID. 8001104.

[16] M. Sieger *et al.*, "Pulsed laser deposition of thick $BaHfO_3$-doped $YBa_2Cu_3O_{7-\delta}$ films on highly alloyed textured Ni-W tapes," *J. Phys., Conf. Ser.*, vol. 507, no. 2, 2014, Art. ID. 022032.

[17] J. B. Nelson and D. P. Riley, "An experimental investigation of extrapolation methods in the derivation of accurate unit-cell dimensions of crystals," *Proc. Phys. Soc.*, vol. 57, no. 3, pp. 160–177, May 1945.

[18] R. Nast *et al.*, "Influence of laser striations on the properties of coated conductors," *J. Phys., Conf. Ser.*, vol. 507, no. 2, 2014, Art. ID. 022023.

[19] International Centre for Diffraction Data, pdf card 00-024-0102 $(BaHfO_3)$.

[20] International Centre for Diffraction Data, pdf card 00-041-1105 (Y_2O_3).

[21] J. Wu *et al.*, "The effect of lattice strain on the diameter of $BaZrO_3$ nanorods in epitaxial $YBa_2Cu_3O_{7-\delta}$ films," *Supercond. Sci. Technol.*, vol. 27, no. 4, Mar. 2014, Art. ID. 044010.

[22] H. Kai *et al.*, "The effect of growth temperature on c-axis-correlated pinning centers in PLD- $ErBa_2Cu_3O_{7-\delta}$ films with $Ba(Er_{0.5}Nb_{0.5})O_3$," *Supercond. Sci. Technol.*, vol. 23, no. 2, Dec. 2010, Art. ID. 025017.

[23] A. Kiessling *et al.*, "Nanocolumns in $YBa_2Cu_3O_{7-x}/BaZrO_3$ quasi-multilayers: Formation and influence on superconducting properties," *Supercond. Sci. Technol.*, vol. 24, no. 5, Mar. 2011, Art. ID. 055018.

[24] B. Maiorov *et al.*, "Synergetic combination of different types of defect to optimize pinning landscape using $BaZrO_3$-doped $YBa_2Cu_3O_7$," *Nat. Mater.*, vol. 8, no. 5, pp. 398–404, Apr. 2009.

[25] L. Fernandez *et al.*, "Influence of the grain boundary network on the critical current of $YBa_2Cu_3O_7$ films grown on biaxially textured metallic substrates," *Phys. Rev. B, Condens. Matter*, vol. 67, no. 5, Feb. 2003, Art. ID. 052503.

[26] D. Verebelyi *et al.*, "Low angle grain boundary transport in $YBa_2Cu_3O_{7-\delta}$ coated conductors," *Appl. Phys. Lett.*, vol. 76, no. 13, pp. 1755–1757, Mar. 2000.